

Measuring both magnitude and sign of the orbital angular momentum of light in a Laguerre-Gaussian rotational-cavity system

Zhucheng Zhang,¹ Yi-Ping Wang,² and Xiaoguang Wang^{1,3*}

¹*Zhejiang Institute of Modern Physics, Department of Physics, Zhejiang University, Hangzhou 310027, China*

²*College of Science, Northwest A&F University, Yangling 712100, China*

³*Graduate School of China Academy of Engineering Physics, Beijing 100193, China*

(Dated: April 22, 2022)

The orbital angular momentum (OAM) intrinsically carried by vortex beams has great application prospects due to its theoretically unbounded and orthogonal modes. Here, we propose a scheme to measure OAM including its magnitude and sign in a Laguerre-Gaussian (LG) rotational-cavity system, which consists of two input couplers and a rotating mirror. We show that since the effective cavity detuning in the traditional single LG cavity is only related to the magnitude of OAM, but not to its sign, only the magnitude of OAM can be measured based on the shift of the transmission spectrum of the probe field. In the double LG cavity, however, the effective cavity detuning varies with the magnitude and sign of OAM, which causes the spectral shift to be directional for different signs of OAM, thus we can simultaneously measure both of them, in which the measurable topological charge value can reach to ± 50 . Our scheme can not only measure a wide range of OAM, but also can distinguish its sign, which is a significant improvement for measuring OAM based on LG rotational-cavity system, and can also expand its application prospects in the field of quantum sensing.

I. INTRODUCTION

Vortex beams, such as Laguerre-Gaussian (LG) beam, possess an azimuthal phase structure $e^{il\psi}$, which can carry a well-defined orbital angular momentum (OAM) of $l\hbar$ per photon, with ψ and l being its azimuthal angle and topological charge value [1, 2]. This type of beams can be generated by diffracting a non-helical beam off a spiral phase plate [3, 4] or off a computer-generated hologram [5, 6]. Recently, the generation and detection of OAM-tunable vortex microlaser on the photonic chip were realized [7, 8]. Due to their quantized OAM and their dynamic characteristics, these helically phased beams are widely used in many fields, such as quantum information technologies [9], optical communications [10, 11], optical trapping [12], optical tweezers [13, 14], and so on. Thus, it is of great importance to measure OAM of vortex beams (or its topological charge value) accurately, including both the magnitude and the sign.

To measure OAM of vortex beams, in general, we can analyze the related interference patterns directly, for example, the interference pattern between the spiral wave front and a flat wave front [15], or the interference pattern between a vortex beam and its mirror image [16]. With the use of a triangular aperture and an annular aperture, the measurement of the topological charge value with $l = \pm 7$ and $|l| = 9$ based on diffraction pattern were also reported [17, 18]. Besides, the highest measurable value of the topological charge was raised to ± 25 by using annular gratings [19]. Recently, based on optomechanically induced transparency (OMIT) [20, 21], a quantum interference effect like electromagnetically induced transparency occurred in multilevel atoms [22], a wide range

of OAM with the topological charge value ranging from 0 to 42 can be measured in theory with a LG rotational-cavity system [23], but this scheme cannot distinguish the sign of OAM.

In this paper, we propose a scheme to measure both magnitude and sign of OAM in a LG rational-cavity system. LG rational-cavity system was first proposed by Bhattacharya and Meystre to trap and cool the rotational motion of a mirror [24]. In this type of cavity optomechanical system, the intracavity radiation field can exchange linear as well as angular momentum with the mirror, which is the difference from the traditional cavity optomechanical system [25–29]. And later, many interesting physical effects have been also studied, such as the entanglement phenomenon based on LG rotational-cavity system [30–32], the ground-state cooling of rotating mirror in the unresolved sideband regime [33], and OMIT [23, 34]. However, the measurement of OAM including the magnitude and the sign in LG rational-cavity system has not been reported, which will have wide applications in precision measurement, and will also expand the application prospects of LG rational-cavity system.

In our scheme, LG rational-cavity system consists of two input couplers and a rotating mirror. We show that the effective cavity detuning of our system varies with the magnitude and sign of OAM simultaneously, which is different from that of traditional single LG rational-cavity system [23, 24]. In single LG rational-cavity system, the effective cavity detuning is only related to the magnitude of OAM but not to its sign, so with the shift of the OMIT window in Ref. [23], only the magnitude of OAM can be measured. In our system, however, both the magnitude and sign of OAM can be measured based on the spectral shift, in which the measurable topological charge value can reach to ± 50 . Besides, compared to single LG rational-cavity system, we observe an OMIT window similar to the Fano resonance, meanwhile we can

* xgwang1208@zju.edu.cn

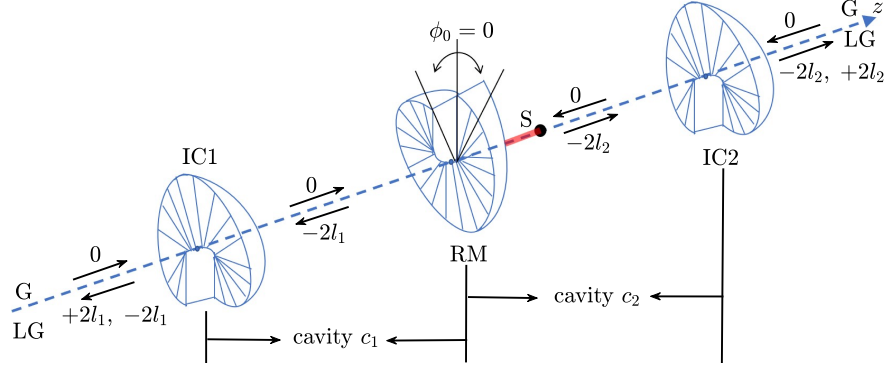


FIG. 1. Arrangement for measuring the orbital angular momentum of light in the Laguerre-Gaussian (LG) rotational-cavity system, in which the two input couplers (IC1, IC2) are partially transparent and rigidly fixed, but the rotating mirror (RM) is perfectly reflective and rotates about the cavity axis z (with angular equilibrium position $\phi_0 = 0$) on a support S . This support is assumed to be small enough so that its effects on cavity c_2 can be neglected. The two input couplers and the rotating mirror are all spiral phase elements. Input fields injected to the system are Gaussian (G) fields with topological charge 0, and the charge on the LG beams at various points has been indicated.

also realize a fully switchable light switch in our system.

This paper is organized as follows. In Sec. II, we introduce our system model and derive the dynamical equation. In Sec. III, we discuss in detail the transmission spectrum of the probe field in the double LG rotational cavity, and compare it with the case of single LG rotational cavity. In Sec. IV, we propose our scheme to measure the magnitude and sign of OAM. Finally, we summarize our conclusions in Sec. V.

II. THEORETICAL MODEL

We consider a Laguerre-Gaussian (LG) rotational-cavity system shown in Fig. 1, which consists of two input couplers (IC1 and IC2) and a rotating mirror (RM). IC1 (IC2) and RM are all spiral phase elements, which can modify the azimuthal structure of laser beams [3, 4]. IC1 (IC2) is partially transparent and rigidly fixed, but RM is perfectly reflective and rotates about the cavity axis z (with angular rotation frequency ω_ϕ), which can be seen as a thin disk with the moment of inertia $I = MR^2/2$ (M and R being its mass and radius). In what follows, we assume that the input fields injected to the system are all Gaussian (G) fields with topological charge 0, whose charge does not change when passing through IC1 or IC2 while the reflected components get charged to $2l_{1,2}$. In addition, RM can remove a topological charge $2l_{1,2}$ from the beams corresponding to cavity c_1 and cavity c_2 . The related cavity conditions have been discussed in detail in Refs. [24, 30, 31].

In our scheme, the two cavities are assumed to be identical, with the same resonance frequency ω_c and decay rate κ . Besides, cavity c_1 is driven by a strong driving field of frequency ω_1 and amplitude ϵ_1 and probed by a weak probe field of frequency ω_p and amplitude

ϵ_p . Meanwhile, another driving field of frequency ω_2 and amplitude ϵ_2 is injected to cavity c_2 . In a rotating frame with respect to $U = \exp[-i(\omega_1 c_1^\dagger c_1 + \omega_2 c_2^\dagger c_2)t/\hbar]$, the Hamiltonian of system can be written as

$$H = \hbar(\Delta_{c1} c_1^\dagger c_1 + \Delta_{c2} c_2^\dagger c_2) + \frac{L_z^2}{2I} + \frac{1}{2} I \omega_\phi^2 \phi^2 \\ + \hbar(g_1 c_1^\dagger c_1 - g_2 c_2^\dagger c_2) \phi \\ + i\hbar[(\epsilon_1 + \epsilon_p e^{-i\Omega t}) c_1^\dagger - \text{H.c.}] + i\hbar(\epsilon_2 c_2^\dagger - \text{H.c.}), \quad (1)$$

in which c_1 (c_1^\dagger) and c_2 (c_2^\dagger) are the bosonic annihilation (creation) operators of the two cavity modes, respectively, satisfying the commutation relation $[c_{1,2}, c_{1,2}^\dagger] = 1$. $\Delta_{c1,2} = \omega_c - \omega_{1,2}$ and $\Omega = \omega_p - \omega_1$ are the frequency detunings of the driving fields from the cavity resonance and the probe field. L_z and ϕ denote the angular momentum of RM about the cavity axis z and angular displacement with the commutation relation $[L_z, \phi] = -i\hbar$. $g_{1,2} = cl_{1,2}/L$ characterize the optorotational coupling between two LG cavity modes and RM [24, 30, 31], respectively, with c and L being the speed of light in vacuum and the length of the cavity. The last two terms describe the coupling between the input fields and the two cavity modes with amplitudes $\epsilon_{1,2} = \sqrt{2\kappa P_{1,2}/\hbar\omega_{1,2}}$ and $\epsilon_p = \sqrt{2\kappa P_p/\hbar\omega_p}$. $P_{1,2,p}$ is the corresponding powers of input fields.

Our scheme focuses on the mean response of the system to the probe field, so we consider the mean-value equations of the system, which can be obtained by deriving the Heisenberg equations of the system operators as well as adding the corresponding damping terms. By using the factorization assumption $\langle AB \rangle = \langle A \rangle \langle B \rangle$ [20], the mean value equations of the system operators can be

derived as follows,

$$\left\langle \frac{dc_1}{dt} \right\rangle = -[\kappa + i(\Delta_{c1} + g_1 \langle \phi \rangle)] \langle c_1 \rangle + \epsilon_1 + \epsilon_p e^{-i\Omega t}, \quad (2)$$

$$\left\langle \frac{dc_2}{dt} \right\rangle = -[\kappa + i(\Delta_{c2} - g_2 \langle \phi \rangle)] \langle c_2 \rangle + \epsilon_2, \quad (3)$$

$$\begin{aligned} \left\langle \frac{d^2\phi}{dt^2} \right\rangle = & -\gamma_\phi \left\langle \frac{d\phi}{dt} \right\rangle - \omega_\phi^2 \langle \phi \rangle \\ & - \frac{\hbar}{I} \left(g_1 \langle c_1^\dagger \rangle \langle c_1 \rangle - g_2 \langle c_2^\dagger \rangle \langle c_2 \rangle \right), \end{aligned} \quad (4)$$

in which γ_ϕ is the damping rate of RM.

The above mean value equations are nonlinear equations, but it can be solved by using the perturbation method due to the fact that the driving fields are much stronger than the probe field. By setting $\langle O \rangle = O_s + \delta O$ ($O = c_{1,2}, L_z, \phi$), one can obtain the steady-state values of the corresponding dynamical variables as

$$\phi_s = \frac{-g_1 \hbar |c_{1s}|^2 + g_2 \hbar |c_{2s}|^2}{I \omega_\phi^2}, \quad L_{zs} = 0, \quad (5)$$

$$c_{1s} = \frac{\epsilon_1}{\kappa + i\Delta_1}, \quad c_{2s} = \frac{\epsilon_2}{\kappa + i\Delta_2}, \quad (6)$$

$$\begin{aligned} \Delta_1 = & \Delta_{c1} + g_1 \phi_s \\ = & \left(\Delta_{c1} - \frac{g_1^2 \hbar |c_{1s}|^2}{I \omega_\phi^2} \right) + \frac{g_1 g_2 \hbar |c_{2s}|^2}{I \omega_\phi^2}, \end{aligned} \quad (7)$$

$$\Delta_2 = \Delta_{c2} - g_2 \phi_s. \quad (8)$$

in which Δ_1 (Δ_2) represents the effective detuning of cavity c_1 (c_2) from the driving fields. One can find that the effective detuning of cavity c_1 can be modulated effectively by cavity c_2 . Besides, this modulation can be improved if we choose a cavity with higher cavity finesse and stronger driving power, as well as a mirror with smaller mass and size. Meanwhile, the resonantly driven cavity c_2 can also greatly enhance its modulation effect on cavity c_1 .

Besides, the equations of the corresponding perturbation terms can be derived as follows,

$$\frac{d\delta c_1}{dt} = -(\kappa + i\Delta_1) \delta c_1 - i g_1 \delta \phi (c_{1s} + \delta c_1) + \epsilon_p e^{-i\Omega t}, \quad (9)$$

$$\frac{d\delta c_2}{dt} = -(\kappa + i\Delta_2) \delta c_2 + i g_2 \delta \phi (c_{2s} + \delta c_2), \quad (10)$$

$$\begin{aligned} \frac{d^2\delta\phi}{dt^2} = & -\gamma_\phi \frac{d\delta\phi}{dt} - \omega_\phi^2 \delta\phi \\ & - \frac{\hbar g_1}{I} (c_{1s}^* \delta c_1 + \delta c_1^* c_{1s} + \delta c_1^* \delta c_1) \\ & + \frac{\hbar g_2}{I} (c_{2s}^* \delta c_2 + \delta c_2^* c_{2s} + \delta c_2^* \delta c_2). \end{aligned} \quad (11)$$

The above equations of the perturbation terms can be solved by applying the ansatz, i.e., $\delta O = O_+ e^{-i\Omega t} + O_- e^{i\Omega t}$, then, one can get the solution of c_{1+} , which corresponds to the response of the system to the probe field

[20, 35].

$$c_{1+} = \frac{-i\epsilon_p [N_1 g_1^2 \hbar + 2N_2 \Delta_2 g_2^2 \hbar D_1(\Omega) + I D_2(\Omega)]}{2N_1 \Delta_1 g_1^2 \hbar + 2N_2 \Delta_2 g_2^2 \hbar D_3(\Omega) + I D_4(\Omega)}, \quad (12)$$

with

$$D_1(\Omega) = \frac{\Delta_1 + \Omega + i\kappa}{\Delta_2^2 + (\kappa - i\Omega)^2}, \quad (13)$$

$$D_2(\Omega) = (\Delta_1 + \Omega + i\kappa)(\Omega^2 - \omega_\phi^2 + i\gamma_\phi \Omega), \quad (14)$$

$$D_3(\Omega) = \frac{\Delta_1^2 + (\kappa - i\Omega)^2}{\Delta_2^2 + (\kappa - i\Omega)^2}, \quad (15)$$

$$D_4(\Omega) = [\Delta_1^2 + (\kappa - i\Omega)^2](\Omega^2 - \omega_\phi^2 + i\gamma_\phi \Omega). \quad (16)$$

Then according to the standard input-output relation [36], i.e., $c_{1out}(t) = c_{1in}(t) - \sqrt{2\kappa} c_1(t)$, with c_{1in} and c_{1out} being the input and output operators of cavity c_1 , respectively, the expectation value of the output field can be written as [20, 35]

$$\begin{aligned} \langle c_{1out} \rangle = & \left(\frac{\epsilon_1}{\sqrt{2\kappa}} - \sqrt{2\kappa} c_{1s} \right) e^{-i\omega_1 t} \\ & + \left(\frac{\epsilon_p}{\sqrt{2\kappa}} - \sqrt{2\kappa} c_{1+} \right) e^{-i\omega_p t} - \sqrt{2\kappa} c_{1-} e^{-i(2\omega_1 - \omega_p)t}, \end{aligned} \quad (17)$$

which clearly shows that in terms of the input probe amplitude, the transmission of probe field can be defined as

$$T = \left| \frac{\epsilon_p / \sqrt{2\kappa} - \sqrt{2\kappa} c_{1+}}{\epsilon_p / \sqrt{2\kappa}} \right|^2 = |1 - 2\kappa c_{1+} / \epsilon_p|^2. \quad (18)$$

III. TRANSMISSION SPECTRUM OF THE PROBE FIELD IN THE DOUBLE LG ROTATIONAL CAVITY

In this section, we will study the response of double LG rotational cavity to the probe field, and compare it with the case of single LG rotational cavity. The parameters used in the numerical simulation of our paper are chosen from Refs. [24, 30, 31]. For RM, the radius $R = 10\mu\text{m}$, the mass $M = 100\text{ng}$, the angular frequency $\omega_\phi = 2\pi \times 10\text{MHz}$, and the mechanical quality factor $Q_\phi = 2 \times 10^6$. For cavity, the cavity length $L = 5\text{mm}$, the cavity finesse $F = 5 \times 10^4$, and cavity c_1 is driven with red-detuned driving (i.e., $\Delta_{c1} = \omega_\phi$, and the frequency ω_1 of driving field is $2\pi c / \lambda_1$ with wavelength $\lambda_1 = 1064\text{nm}$); meanwhile, cavity c_2 is driven resonantly with the effective detuning $\Delta_2 = 0$, which can be achieved by the use of electronic feedback. It is worth mentioning that the electronic feedback used in cavity c_2 is carried out routinely by many theoretical and experimental works [24, 30, 31, 37], which can set the net detuning of cavity independently of radiation pressure and can also avoid the occurrence of bistability. We would also point out

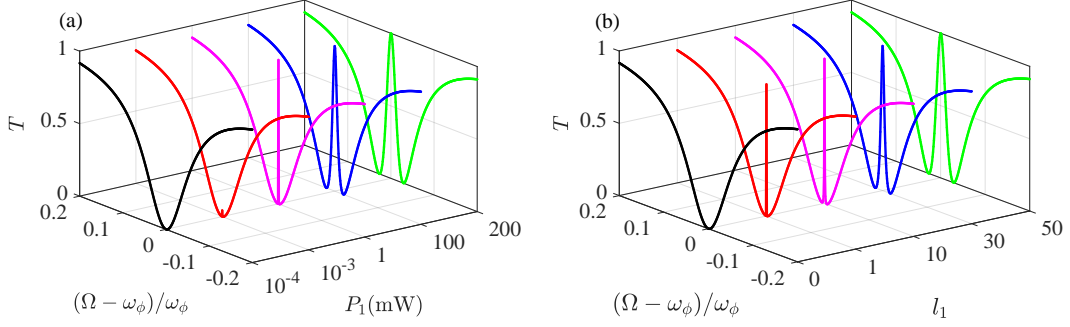


FIG. 2. Transmission spectrum of the probe field in single LG rotational cavity as a function of the normalized detuning $(\Omega - \omega_\phi)/\omega_\phi$ for (a) different driving powers ($P_1 = 0.1\mu\text{W}$, $1\mu\text{W}$, 1mW , 100mW and 200mW), and (b) different orbital angular momentum of LG light ($l_1 = 0, 1, 10, 30$ and 50). The parameters are: (a) $l_1 = 50$, (b) $P_1 = 200\text{mW}$, and other parameters are: $F = 5 \times 10^4$, $L = 5\text{mm}$, $\omega_\phi = 2\pi \times 10\text{MHz}$, $Q_\phi = 2 \times 10^6$, $R = 10\mu\text{m}$, $M = 100\text{ng}$, $\lambda_1 = 1064\text{nm}$, $\omega_1 = 2\pi c/\lambda_1$, and $\Delta_{c1} = \omega_\phi$.

that cavity c_1 with red-detuned driving can exhibit bistability for strong enough driving field [38, 39], however, the parameters used in our paper are chosen in the area of monostability.

At first, we analyze the transmission characteristics of probe field in single LG rotational cavity. As shown in Fig. 2, we plot the transmission spectrum of probe field in single LG rotational cavity as a function of the normalized detuning $(\Omega - \omega_\phi)/\omega_\phi$. For a fixed topological charge l_1 of LG light, one can observe from the curves of Fig. 2(a) that with the increase of the power P_1 of driving field, an OMIT window can occur in the transmission spectrum of probe field. Besides, for a fixed power of driving field, the OMIT window can also appear and its width becomes wider and wider when we increase the topological charge of LG light [see Fig. 2(b)]. Thus, based on the correlation between the window width and the topological charge, OAM can be measured in principle as shown in Ref. [23]. But, we would point out that only the magnitude of OAM can be measured via this method. This is due to the fact that the effective cavity detuning Δ_1 of single LG rotational cavity is only related to the magnitude of OAM and not to its sign, which can be seen from Eq. (7) [this equation is simplified as $\Delta_1 = \Delta_{c1} - c^2 l_1^2 \hbar |c_{1s}|^2 / I \omega_\phi^2 L^2$ for single LG rotational cavity].

Now we study the transmission characteristics of probe field in the double LG rotational cavity. The transmission spectrum of probe field in the double LG rotational cavity is plotted as a function of the normalized detuning $(\Omega - \omega_\phi)/\omega_\phi$, as shown in Figs. 3(a) and 3(b). From the curves of Fig. 3(a), one can see that for a weak driving field with power $P_1 = 0.1\mu\text{W}$, the Lorentzian-shaped transmission spectrum originally located at the resonance frequency $\Omega \approx \omega_\phi$ shifts obviously with the increase of the driving field of cavity c_2 . What's more, for different sign of OAM, the direction of the spectral shift is just opposite. Specifically, for the topological charge $l_1 = 50$, the transmission spectrum shifts to the right,

but for $l_1 = -50$, it shifts to the left. Thus, this spectral shift can be served as a fully switchable light switch through adjusting the power of driving field, as shown in Fig. 3(c). Besides, one can find from the curves of Fig. 3(b) that for a stronger driving field with power $P_1 = 100\text{mW}$, a symmetrical OMIT window occurs in the resonance frequency $\Omega \approx \omega_\phi$, but this symmetry is broken once cavity c_2 is introduced, then an asymmetry window similar to the Fano resonance can be observed. Like the Lorentzian-shaped transmission spectrum [(see Fig. 3(a))], the asymmetric transparency window also has a strong correlation with the magnitude and sign of OAM simultaneously. This correlation can be understood based on the dependence of the effective detuning of cavity c_1 on the cavity c_2 . As shown in Fig. 3(d), we plot the normalized cavity detuning $(\Delta_1 - \omega_\phi)/\omega_\phi$ as a function of the driving power P_2 . From Fig. 3(d), one can clearly see that the effective detuning of cavity c_1 strongly depends on the driving power of cavity c_2 , in which different signs of OAM change in reverse with the increase of the driving field. Furthermore, one can also find that the value of the normalized cavity detuning is consistent with the position of the resonance valley of the transmission spectrum. The above shift of the transmission spectrum induced by cavity c_2 gives us the inspiration of measuring both the magnitude and sign of OAM simultaneously.

IV. MEASUREMENT OF THE MAGNITUDE AND SIGN OF ORBITAL ANGULAR MOMENTUM

In this section, we apply the spectral shift induced by cavity c_2 to measure the magnitude and sign of OAM simultaneously. As shown in Fig. 4(a), we plot the transmission spectrum of the probe field in the double LG rotational cavity as a function of the normalized detuning $(\Omega - \omega_\phi)/\omega_\phi$ for different OAM. From the curves, one can observe that for a fixed driving power of cavity c_2 ,

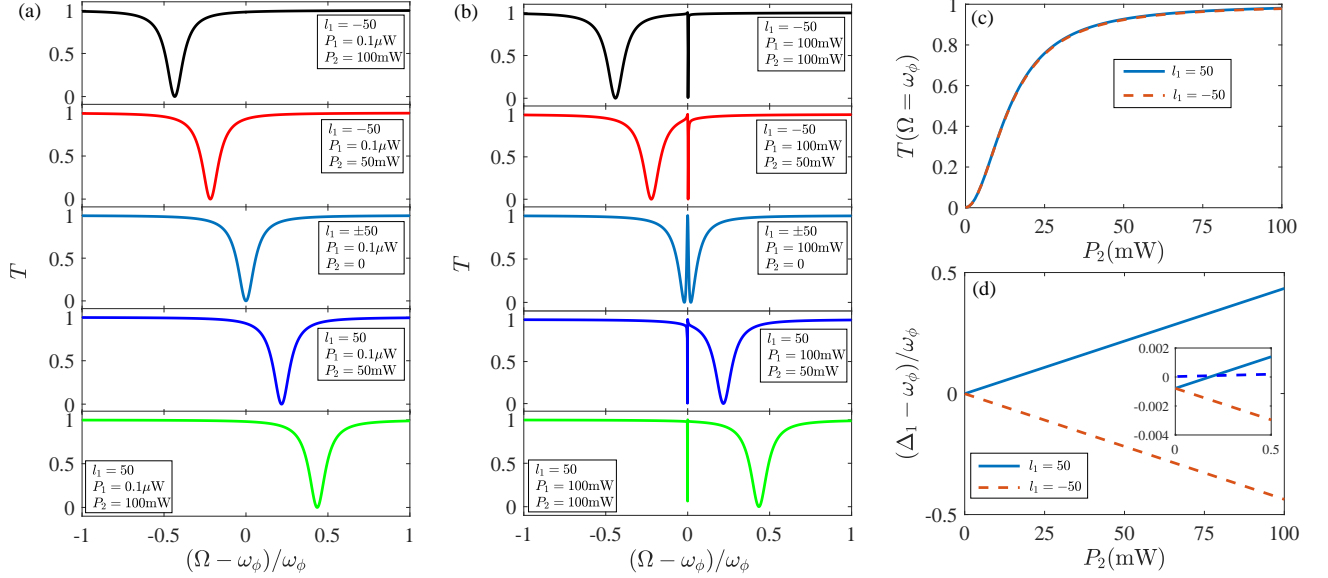


FIG. 3. (a), (b) Transmission spectrum of the probe field in the double LG rotational cavity as a function of the normalized detuning $(\Omega - \omega_\phi)/\omega_\phi$ for different driving powers P_2 of cavity c_2 ($P_2 = 0, 50\text{mW}, 100\text{mW}$), in which black curve and red curve represent $l_1 = -50$, and magenta curve, blue curve and green curve represent $l_1 = 50$. (c) Transimission of the probe field at resonance as a function of the driving power of cavity c_2 . (d) Normalized cavity detuning as a function of the driving power of cavity c_2 , in which the inset shows that due to the presence of optorotational coupling of cavity c_1 , the value of normalized cavity detuning isnt zero. Parameters are: (a), (c) $P_1 = 0.1\mu\text{W}$, $l_2 = 100$; (b), (d) $P_1 = 100\text{mW}$, $l_2 = 100$; and other parameters are the same as in Fig. 2 except $\Delta_2 = 0$.

the Lorentzian-shaped transmission spectrum can show a significant spectral shift when we increase the magnitude of OAM. Specifically, for OAM with positive sign, the resonance valley of the transmission spectrum shifts to the right with the increase of the magnitude of OAM, and for OAM with negative sign, the situation is exactly the opposite. Thus, based on the correlation between position of the resonance valley and OAM, we can measure both the magnitude and sign of OAM simultaneously. The position of the resonance valley can be determined by the following conditions,

$$\left. \frac{dT}{d\Omega} \right|_{\Omega=\Omega_0} = 0, \quad \left. \frac{d^2T}{d\Omega^2} \right|_{\Omega=\Omega_0} > 0, \quad (19)$$

with $x = (\Omega_0 - \omega_\phi)/\omega_\phi$ corresponding to the position of the resonance valley. In order to clearly show this correlation, we plot the position of the resonance valley as a function of the magnitude and sign of OAM, as shown in Fig. 4(b), in which the topological charge value l_1 changes in integer. Figure 4(b) shows that there is an almost linear relationship between the position of resonance valley and the magnitude of OAM. Besides, for the positive and negative signs of OAM, the position is basically symmetrical about the resonance frequency $\Omega \approx \omega_\phi$, which is different from Fig. 5 of Ref. [23], where only the magnitude of OAM can be measured. This spectral shift with the magnitude and sign of OAM can also be understood with the effective detuning of cavity c_1 , as shown in Fig. 4(c).

One can find that the trend of the normalized cavity detuning with OAM (including its magnitude and sign) is consistent with Fig. 4(b).

Thus, based on the above analysis, compared with other schemes [17–19], our proposal can measure a wider range of OAM with the measurable topological charge value ± 50 . Meanwhile, through measuring the position of the resonance valley in the double LG rotational cavity, our proposal can distinguish the sign of OAM compared to the case of single LG rotational cavity of Ref. [23]. Finally, we would point out that the sensitivity of our scheme can be improved when the effective detuning of cavity c_1 is further modulated by cavity c_2 , which can be seen from Eq. (7). We believe that our scheme provides an effective method for the measurement of OAM including magnitude and sign, and can work better with the rapid development of experimental technology.

V. CONCLUSIONS

In summary, we have investigated the transmission characteristics of the probe field in the double LG rotational cavity and showed that the effective cavity detuning depends on the magnitude and sign of OAM simultaneously, which is different from the case of single LG rotation cavity. Moreover, we found that the transmission spectrum of the probe field has a strong correlation

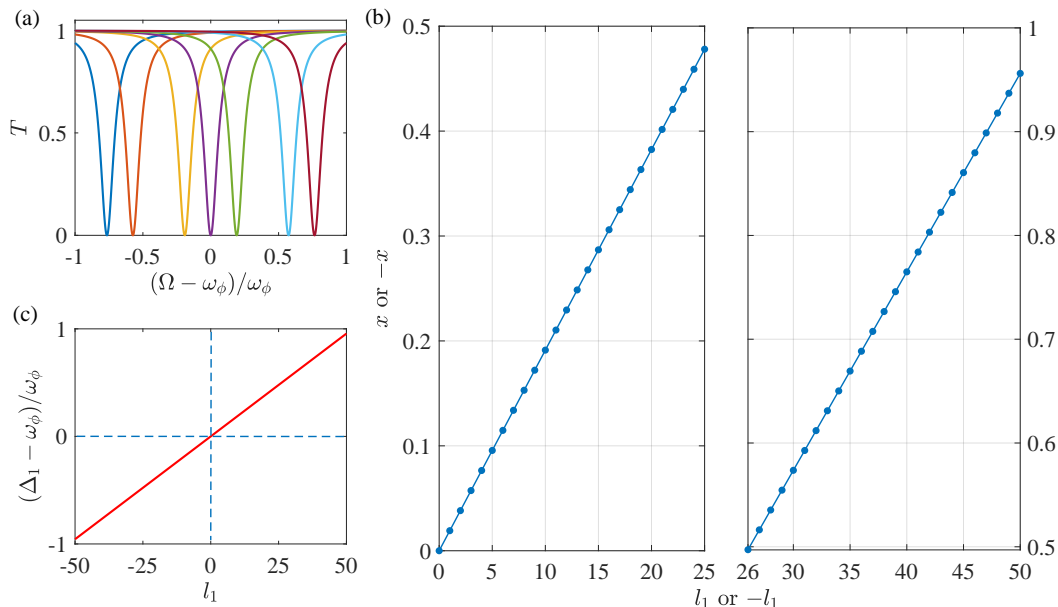


FIG. 4. (a) Transmission spectrum of the probe field in the double LG rotational cavity as a function of the normalized detuning $(\Omega - \omega_\phi)/\omega_\phi$ for different orbital angular momentum (from left to right: $l_1 = -40, -30, -10, 0, 10, 30$, and 40). (b) Position of the resonance valley of the transmission spectrum as a function of orbital angular momentum. (c) Normalized cavity detuning as a function of the orbital angular momentum. Parameters are: $P_1 = 0.1\mu\text{W}$, $P_2 = 220\text{mW}$, $l_2 = 100$, and other parameters are the same as in Fig. 2 except $\Delta_2 = 0$.

with the magnitude and sign of OAM. Specifically, for different magnitudes of OAM, the transmission spectrum can show an obvious spectral shift, meanwhile, the spectral shift is directional for different signs of OAM. Thus, based on this feature, we propose a scheme to measure OAM including the magnitude and the sign, in which the measurable topological charge is up to ± 50 . This work provides an effective method to measure both magnitude and sign of OAM, and also expands the application prospects of the LG rotational-cavity system in quantum sensing.

ACKNOWLEDGMENTS

This work was supported by the National Key Research and Development Program of China (Grants No. 2017YFA0304202 and No. 2017YFA0205700), the National Natural Science Foundation of China (NSFC) (Grants No. 11875231 and No. 11935012), and the Fundamental Research Funds for the Central Universities through Grant No. 2018FZA3005.

-
- [1] J. F. Nye and M. V. Berry, Dislocations in wave trains, *Proc. R. Soc. A* **336**, 165 (1974).
 - [2] L. Allen, M. W. Beijersbergen, R. J. C. Spreeuw, and J. P. Woerdman, Orbital angular momentum of light and the transformation of laguerre-gaussian laser modes, *Phys. Rev. A* **45**, 8185 (1992).
 - [3] M. W. Beijersbergen, R. P. C. Coerwinkel, M. Kristensen, and J. P. Woerdman, Helical-wavefront laser beams produced with a spiral phaseplate, *Opt. Commun.* **112**, 321 (1994).
 - [4] S. S. R. Oemrawsingh, E. R. Eliel, J. P. Woerdman, E. J. K. Verstegen, J. G. Kloosterboer, and G. W. T. Hooft, Half-integral spiral phase plates for optical wavelengths, *J. Opt. A: Pure Appl. Opt.* **6**, S288 (2004).
 - [5] V. Y. Bazhenov, M. S. Soskin, and M. V. Vasnetsov, Screw dislocations in light wavefronts, *J. Mod. Opt.* **39**, 985 (1992).
 - [6] I. V. Basistiy, V. Y. Bazhenov, M. S. Soskin, and M. V. Vasnetsov, Optics of light beams with screw dislocations, *Opt. Commun.* **103**, 422 (1993).
 - [7] Z. Zhang *et al.*, Tunable topological charge vortex micro-laser, *Science* **368**, 760763 (2020).
 - [8] Z. Ji *et al.*, Photocurrent detection of the orbital angular momentum of light, *Science* **368**, 763767 (2020).
 - [9] D. S. Ding *et al.*, Quantum storage of orbital angular momentum entanglement in an atomic ensemble, *Phys. Rev. Lett.* **114**, 050502 (2015).
 - [10] J. Wang *et al.*, Terabit free-space data transmission employing orbital angular momentum multiplexing, *Nat. Photon.* **6**, 488 (2012).
 - [11] N. Bozinovic *et al.*, Terabit-scale orbital angular momentum mode division multiplexing in fibers, *Science* **340**, 1545 (2013).

- [12] M. Chen, M. Mazilu, Y. Arita, E. M. Wright, and K. Dhollakia, Dynamics of microparticles trapped in a perfect vortex beam, *Opt. Lett.* **38**, 4919 (2013).
- [13] M. J. Padgett and R. Bowman, Tweezers with a twist, *Nat. Photon.* **5**, 343 (2011).
- [14] M. Gecevicius, R. Drevinskas, M. Beresna, and P. G. Kazansky, Single beam optical vortex tweezers with tunable orbital angular momentum, *Appl. Phys. Lett.* **104**, 231110 (2014).
- [15] M. Harris, C. A. Hill, and J. M. Vaughan, Optical helices and spiral interference fringes, *Opt. Commun.* **106**, 161 (1994).
- [16] M. Harris, C. A. Hill, P. R. Tapster, and J. M. Vaughan, Laser modes with helical wave fronts, *Phys. Rev. A* **49**, 3119 (1994).
- [17] J. M. Hickmann, E. J. S. Fonseca, W. C. Soares, and S. Chavezcerda, Unveiling a truncated optical lattice associated with a triangular aperture using light's orbital angular momentum, *Phys. Rev. Lett.* **105**, 053904 (2010).
- [18] C. S. Guo, L. L. Lu, and H. T. Wang, Characterizing topological charge of optical vortices by using an annular aperture, *Opt. Lett.* **34**, 3686 (2009).
- [19] S. Zheng and J. Wang, Measuring orbital angular momentum (oam) states of vortex beams with annular gratings, *Sci. Reports* **7**, 40781 (2017).
- [20] G. S. Agarwal and S. Huang, Electromagnetically induced transparency in mechanical effects of light, *Phys. Rev. A* **81**, 041803(R) (2010).
- [21] S. Weis, R. Riviere, S. Deleglise, E. Gavartin, O. Arcizet, A. Schliesser, and T. J. Kippenberg, Optomechanically induced transparency, *Science* **330**, 1520 (2010).
- [22] S. E. Harris, Electromagnetically induced transparency, *Phys. Today* **50**, 36 (1997).
- [23] J. X. Peng, Z. Chen, Q. Z. Yuan, and X. L. Feng, Optomechanically induced transparency in a laguerre-gaussian rotational-cavity system and its application to the detection of orbital angular momentum of light fields, *Phys. Rev. A* **99**, 043817 (2019).
- [24] M. Bhattacharya and P. Meystre, Using a laguerre-gaussian beam to trap and cool the rotational motion of a mirror, *Phys. Rev. Lett.* **99**, 153603 (2007).
- [25] M. Aspelmeyer, T. J. Kippenberg, and F. Marquardt, Cavity optomechanics, *Rev. Mod. Phys.* **86**, 1391 (2014).
- [26] C. K. Law, Interaction between a moving mirror and radiation pressure: A hamiltonian formulation, *Phys. Rev. A* **51**, 2537 (1995).
- [27] M. Bhattacharya, H. Uys, and P. Meystre, Optomechanical trapping and cooling of partially reflective mirrors, *Phys. Rev. A* **77**, 033819 (2008).
- [28] Y. Xiao, Y. F. Yu, and Z. M. Zhang, Controllable optomechanically induced transparency and ponderomotive squeezing in an optomechanical system assisted by an atomic ensemble, *Opt. Express* **22**, 17979 (2014).
- [29] Z. Zhang and X. Wang, Photon-assisted entanglement and squeezing generation and decoherence suppression via a quadratic optomechanical coupling, *Opt. Express* **28**, 2732 (2020).
- [30] M. Bhattacharya, P. Giscard, and P. Meystre, Entanglement of a laguerre-gaussian cavity mode with a rotating mirror, *Phys. Rev. A* **77**, 013827 (2008).
- [31] M. Bhattacharya, P. Giscard, and P. Meystre, Entangling the rovibrational modes of a macroscopic mirror using radiation pressure, *Phys. Rev. A* **77**, 030303(R) (2008).
- [32] Z. Chen, J. X. Peng, J. J. Fu, and X. L. Feng, Entanglement of two rotating mirrors coupled to a single laguerre-gaussian cavity mode, *Opt. Express* **27**, 29479 (2019).
- [33] Y. M. Liu, C. H. Bai, D. Y. Wang, T. Wang, M. H. Zheng, H. F. Wang, A. D. Zhu, and S. Zhang, Ground-state cooling of rotating mirror in double-laguerre-gaussian-cavity with atomic ensemble, *Opt. Express* **26**, 6143 (2018).
- [34] J. X. Peng, Z. Chen, Q. Z. Yuan, and X. L. Feng, Double optomechanically induced transparency in a laguerre-gaussian rovibrational cavity, *Phys. Rev. A* **384**, 126153 (2020).
- [35] S. Huang and G. S. Agarwal, Normal-mode splitting and antibunching in stokes and anti-stokes processes in cavity optomechanics: Radiation-pressure-induced four-wave-mixing cavity optomechanics, *Phys. Rev. A* **81**, 033830 (2010).
- [36] C. W. Gardiner and P. Zoller, *Quantum noise: a handbook of Markovian and non-Markovian quantum stochastic methods with applications to quantum optics* (Springer-Verlag, 2004).
- [37] S. Gigan *et al.*, Self-cooling of a micromirror by radiation pressure, *Nature* **444**, 67 (2006).
- [38] J. D. McCullen, P. Meystre, and E. M. Wright, Mirror confinement and control through radiation pressure, *Opt. Lett.* **9**, 193 (1984).
- [39] A. Baas, J. P. Karr, H. Eleuch, and E. Giacobino, Optical bistability in semiconductor microcavities, *Phys. Rev. A* **69** (2004).